

Density functional approach to the description of fluids in contact with bilayers

A. Patrykiewicz,¹ S. Sokółowski,^{1,a)} J. Ilnytskyi,² and Z. Sokółowska³

¹Department for the Modeling of Physico-Chemical Processes, Maria Curie-Skłodowska University, 20-031 Lublin, Poland

²Institute for Condensed Matter Physics, National Academy of Sciences of Ukraine, 1 Svientsitskii Street, 79011 Lviv, Ukraine

³Institute of Agrophysics, Polish Academy of Sciences, Doświadczalna 4, 20290 Lublin 27, Poland

(Received 29 March 2010; accepted 2 June 2010; published online 24 June 2010)

We discuss an application of a density functional approach to describe a bilayer, or a simplified model of a membrane, that is built of tethered chain molecules. The bilayer integrity is maintained by tethering chain particles to two common sheets. We study the structure of a two-component mixture in contact with the bilayer, as well as the solvation force acting between two bilayers, immersed in a fluid. The fluid is a binary mixture involving the component that can cross freely the bilayer and the second impenetrable component. All the calculations are carried out for athermal system, in which only hard-core interactions are present. © 2010 American Institute of Physics. [doi:10.1063/1.3456263]

I. INTRODUCTION

Recently, density functional approaches have been successfully applied to study several systems containing complex molecules. The investigations reported in the literature have concerned the adsorption of chain^{1–9} and polyatomic molecules of more complex geometry,^{10–13} the description of the formation of tethered brushes on solid surfaces and adsorption of simple fluids on surfaces modified by attached brushes,^{14–21} studies of adsorption in pores modified by pillars,^{22,23} as well as studies of nonuniform polyelectrolytes and the systems involving charged brushes.^{16,24–28} One should also note that a simple model of a layer (or layers) of chain molecules that are terminally joined to a surface can be also used as a crude model of a membrane.^{29–33}

Polymeric membranes play an important role in several important processes such as, for example, oxygen enrichment, hydrogen separation, and carbon dioxide recovery.^{34–36} Moreover, lipid bilayers are of fundamental importance in cellular biology, and model bilayer systems are fascinating physical systems on their own right.^{37–40} A vast majority of studies of systems involving bilayers have been carried out employing different simulation techniques, see, e.g., Refs. 40–48. Simulation models for such membranes have been developed over a range of resolutions, from fully atomistic descriptions to continuous elastic sheets, to address the many different length scales relevant to experimental observations, cf. Refs. 40, 41, and 49 and the references quoted therein. A comprehensive review of different membrane models, involving coarse-grained and particle-based models, has been recently given by Brannigan *et al.*⁴⁰ Among them, the so-called “tethered chain models”^{49–51} are particularly interesting for us. These models maintain bilayer integrity by tethering: the particles can be either bound to each other or to

one or two common sheets. The tethered chain models have been used to investigate chain conformations, depletion forces, and related properties of bilayers.^{33,50,52–54}

In this work we apply a density functional approach to describe solvent-polymeric bilayer system. The bilayer is modeled as composed of two sheets, each sheet built of chain molecules with the heads tethered to a plane. The particular model applied in numerical calculations is athermal, i.e., only hard-core, excluded volume interactions between the chain segments and solution molecules are taken into account. As a result, the behavior of the system is temperature independent. Our principal aim is to point out several possibilities offered by the proposed treatment rather than to try to mimic the behavior of a selected experimental setup. We also consider a system composed of two bilayers. The latter model can be used to mimic the system of pores with partially permeable walls.^{55,56} However, in this work we are also interested in the determination of the solvation force^{57,58} acting between two bilayers.

II. THEORY

We consider the setup depicted in Fig. 1. The system is composed of two bilayers of chain particles at a distance L apart. In the case of the first bilayer the heads (i.e., the segments labeled $J=1$) of chains are tethered to the two planes located at $z=-L/2$ and at $z=-L/2-h_m$, respectively. For the second bilayer these planes are at $z=L/2$ and $z=L/2+h_m$. For simplicity we assume that all the chains are identical and that each chain is built of M tangentially jointed hard spheres of the same diameter σ_C . The total amount of chain is fixed. Moreover, the number of chains in each bilayer that are pinned at each plane is assumed to be the same. Of course, the last assumption is not essential and can be removed.

^{a)}Electronic mail: stefan.sokolowski@gmail.com.

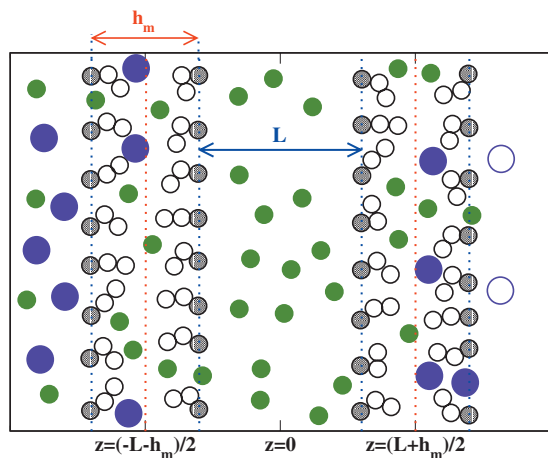


FIG. 1. Schematic representation of the model under study. Dotted blue lines denote the planes, at which the segments (marked as shaded circles) are pinned. The number of the chains pinned at each plane is the same. The free segments are marked by open circles. Green circles represent the molecules of species 1; they can cross the bilayer. Big violet circles denote the molecules of the species 2 that cannot cross the centers of the bilayers (the centers are marked as dotted red lines). The width of the pore formed by two bilayers is L and h_m denotes the width of each bilayer. The system is assumed to be symmetric with respect to $z=0$ plane.

The chain connectivity is ensured by the binding potential between nearest-neighbor segments. The total binding potential V_b is given by²

$$\exp[-\beta V_b(\mathbf{R})] = \prod_{i=1}^{M-1} [\delta(|\mathbf{r}_i - \mathbf{r}_{i+1}|) - \sigma_{(C)}] / 4\pi(\sigma_{(C)})^2. \quad (1)$$

In the above $\mathbf{R} = (\mathbf{r}_1, \mathbf{r}_2, \dots, \mathbf{r}_M)$ is the vector of coordinates of all the segments.

In the case of the first bilayer, extending from $L/2$ to $L/2 + h_m$, see Fig. 1, the first, $J=1$, segment of chains is pinned at $z=L/2$ or at $z=L/2 + h_m$, i.e., it feels a very strong, short-ranged potential,

$$\exp[-\beta v_1^{(C)}(z)] = C\delta(\kappa_1), \quad (2)$$

where $\kappa_1 = z - L/2$ or $\kappa_1 = z - (L/2 + h_m)$. For the second bilayer, however, $\kappa_1 = z - (-L/2)$ or $\kappa_1 = z - (-L/2 - h_m)$. In the above C is a constant, the precise value of which is irrelevant if the total number of grafted chains is fixed.^{17,18,22,23,59} We have already mentioned the number of segments tethered at each plane in two bilayers is the same. Below, this number will be related to the density profile of segments of chain molecules. For the moment we just introduce notation for the parameter describing the number of grafted chains in a single bilayer per unit surface area as R_C .

All the remaining segments, $J=2, 3, \dots, M$, must occupy the space $L/2 \leq z \leq L/2 + h_m$ in the case of the first bilayer (and the space $-L/2 \leq z \leq -L/2 - h_m$ for the second bilayer) To assure that we impose an external potential of the form

$$v_J^{(C)}(z) = \begin{cases} 0 & L/2 \leq z \leq L/2 + h_m \\ \infty & \text{otherwise.} \end{cases} \quad (3)$$

The above equation is related to the first bilayer, a quite analogous equation can be written down for the second bilayer.

The system also contains spherical molecules of the species 1 and 2; they are just hard spheres of the diameters σ_1 and σ_2 , respectively. The interactions between unlike species and between the species 1 and 2 and the chain's segments are also of hard-sphere type with of the additive diameters. The molecules of the type 1 can move freely over the entire system. However, the molecules of the second component, 2, can be found "outside the bilayers" only, see Fig. 1.

In computer simulations the condition for the bilayer permeability can be imposed by taking into account the bilayer density and/or the size of the bilayer's voids.^{40,42} Therefore, during simulation runs the permeability can be "online" modified, depending on the thermodynamic conditions and on the properties of a solution being in contact with the bilayer. No such possibility exists in an equilibrium theory. To assure partial permeability of some components we must *a priori* impose an auxiliary potential field that prevents the molecules of those species to enter certain parts of the system, cf. Refs. 60 and 61. Thus, we assume that

$$v^{(2)}(z) = \begin{cases} \infty & -L/2 - h_m/2 \leq z \leq L/2 + h_m/2 \\ 0 & \text{otherwise,} \end{cases} \quad (4)$$

i.e., the component 2 can be found only "outside" the bilayers, cf. Fig. 1. The external potential acting on the first component is zero everywhere, $v^{(1)}(\mathbf{r}) \equiv 0$. Of course, the last equation is entirely *ad hoc*, in particular, one can consider a model according to which infinite potential barriers are set not at the bilayer centers, but rather at one of their boundaries.

The model used by us can be called the "inner leaflet" model. It mimics some models of lipid bilayers bilayer used in the literature, cf. Refs. 32 and 39. Of course, this model is very simple. The most important limitation of the model results from the assumption that the "heads" of the chains are pinned to two planes [their density distribution is given by the δ -function, cf. Eq. (2)], located at a constant separation. Next, we assume that all the segments can occupy the "inner" space between the two planes. Finally, at the moment we do not consider attractive interactions in the system and limit ourselves to the study of the volume exclusion and chain connectivity effects only.

In order to proceed, let us introduce the notations $\rho^{(C)}(\mathbf{R})$ and $\rho^{(i)}(\mathbf{r})$, $i=1, 2$, for density distributions of chains and spherical species, respectively, and define the segment densities $\rho_{s,j}^{(C)}$ and the total segment density of chains, $\rho_s^{(C)}$ via the relation⁴

$$\rho_s^{(C)}(\mathbf{r}) = \sum_{j=1}^M \rho_{s,j}^{(C)}(\mathbf{r}) = \sum_{j=1}^M \int d\mathbf{R} \delta(\mathbf{r} - \mathbf{r}_j) \rho^{(C)}(\mathbf{R}). \quad (5)$$

To simplify the equations below we also use the notation $\rho_s^{(i)}(\mathbf{r}) \equiv \rho_{s,1}^{(i)}(\mathbf{r}) \equiv \rho^{(i)}(\mathbf{r})$.

The system is studied in the grand canonical ensemble with the constraint of constancy of the number of chain molecules, i.e.,

$$R_C = \int_{-L/2-h_m \leq z \leq -L/2+h_m/2} \rho_{s,1}^{(C)}(z) dz = \int_{L/2-h_m \leq z \leq L/2+h_m/2} \rho_{s,1}^{(C)}(z) dz, \quad (6)$$

as it has already been mentioned. The thermodynamic potential appropriate to describe the system is

$$\mathcal{Y} = F[\rho^{(C)}(\mathbf{R}), \rho^{(1)}(\mathbf{r}), \rho^{(2)}(\mathbf{r})] + \int d\mathbf{r} \sum_{i=1}^2 \rho^{(i)}(\mathbf{r})(v^{(i)}(\mathbf{r}) - \mu) + \sum_{i=1}^M \int d\mathbf{r} \rho_{s,i}^{(C)}(\mathbf{r})(v_i^{(C)}(\mathbf{r})), \quad (7)$$

where $F[\rho^{(C)}(\mathbf{R}), \rho^{(1)}(\mathbf{r}), \rho^{(2)}(\mathbf{r})]$ is the Helmholtz free energy functional.

The expression for $F[\rho^{(C)}(\mathbf{R}), \rho^{(1)}(\mathbf{r}), \rho^{(2)}(\mathbf{r})]$ is taken from the theory outlined in previous works.^{62–65} In particular, the hard-sphere contribution to the free energy functional was evaluated from the Boublik–Moonsori–Carnahan–Starling–Leland equation of state, cf. Ref. 62. The density profile $\rho^{(i)}(\mathbf{r})$, $i=1,2$ and the segment density profiles $\rho_{s,i}^{(C)}(\mathbf{r})$ are obtained by minimizing the functional \mathcal{Y} under constraint (6). For the sake of brevity we do not present the resulting density profile equations, since they are formally identical with those reported in our recent works.^{17,18,22,23}

The solvation force (per unit area) acting between two bilayers is calculated from

$$f_s/kT = - \frac{\partial(\mathcal{Y}/AkT)}{\partial L} - p/kT, \quad (8)$$

where p is the pressure of the bulk system outside the bilayers. Unlike in the case of two plates modified with attached brushes,⁵⁹ f_s comprises the contribution from the molecules located at $-L/2 < z < L/2$ (“inner contribution”) and the contribution from the molecules located outside that range (“outer contribution”). These two contributions are coupled and it is impossible to evaluate them separately without additionally simplifying assumptions.

Below we use the reduced local densities. They are defined as $\rho_s^{(C)*}(z) = \rho_s^{(C)}(z)\sigma_C^3$ and $\rho_s^{(i)*}(z) = \rho_s^{(i)}(z)\sigma_i^3$ for $i=1$ and $i=2$. Also, the individual segment density profiles are $\rho_{s,j}^{(C)*}(z) = \rho_{s,j}^{(C)}(z)\sigma_C^3$. We introduce the abbreviations $\rho_s^{(C,L)*}(z)$ and $\rho_s^{(C,R)*}(z)$ for the segment density profiles that are pinned to the left and the right planes, respectively.

III. RESULTS AND DISCUSSION

We begin with the presentation of examples illustrating the structure of a single model bilayer in a vacuum. The center of the bilayer is located at $z=0$ and thus its delimiting planes are at $z=-h_m/2$ and $z=h_m/2$. Figure 2 shows how the segment density profiles change with increasing $R_C^* = R_C\sigma_C^2$.

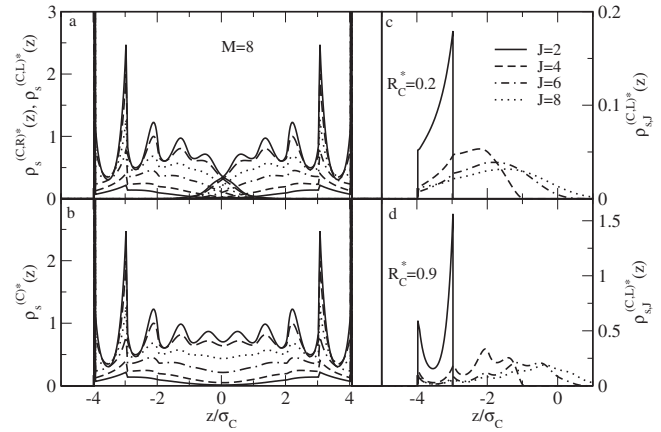


FIG. 2. Total segment density profiles for chains of $M=8$ pinned at the left and the right planes (a) total segment density profiles (b) and the individual segment density profiles for the segments pinned at the left plane, and [(c) and (d)] the segment numbers are given in the figure. The curves from bottom in (a) and (b) are for $R_C=0.1, 0.2, 0.4, 0.6, 0.8$, and 0.9 . The curves in (c) and (d) are for $R_C=0.2$ and 0.9 , respectively.

The calculations have been performed for chains built of $M=8$ segments. The width of the bilayer is $h_m=M\sigma_C$, therefore the numerical value of the average total segment density in the bilayer equals R_C . Part a shows total profiles of segments attached to the “left,” $\rho_s^{(C,L)}(z)$, and “right,” $\rho_s^{(C,R)}(z)$, planes. Part b displays the total segment density profiles $\rho_s^{(C)}(z)$, while parts c and d show examples of the profiles of individual selected segments that are pinned at the left plane and calculated for $R_C^*=0.2$ (part c) and $R_C^*=0.9$ (part d).

At low R_C^* ($R_C^* \leq 0.2$) the chains are coiled and the space at the center of the bilayer remains almost empty. When R_C^* increases the chains become more stretched, but even at the highest value of R_C^* the chains that are tethered at one plane are mostly accumulated within the half of the bilayer adjacent to that plane. This is due the fact that another half-part of the space is occupied by the chains tethered at the opposite plane.

For $M=8$ and at the highest values of R_C^* the total segment density profiles [cf. Fig. 2(b)] show a well-pronounced layered structure. The layering also exhibits individual segment density profiles [Fig. 2(d)], except for the profiles for the most “outer” segments, $J=8$. Because of hard-sphere segment-segment interactions, the effects shown above are entirely entropic. Similar calculations were carried out for much longer chains ($M=22$) and for the bilayer of $h_m=22\sigma_C$ wide, but for the sake of brevity the relevant figures were omitted. We only one that the behavior of the latter system was qualitatively similar as the system shown in Fig. 2.

For bilayers wider than $h_m > 2M\sigma_C$ the layers formed at opposite planes are independent of each other. In such cases the effect of stretching of chains due to increasing R_C^* is obviously more pronounced, compared the cases discussed above. In Fig. 3 we have displayed the total segment density profiles (part a) and individual segment density profiles (parts b and c) for the bilayer formed of chains composed of $M=8$ segments and of the width of $h_m=19\sigma_C$. Because of independence of the chains pinned to the left and right planes, only the profiles at the left plane are shown.

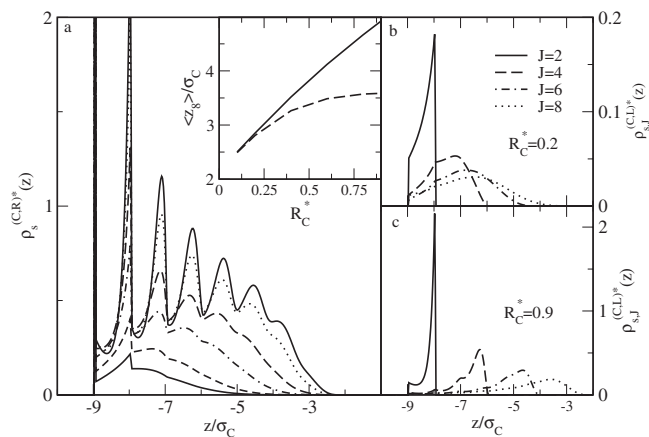


FIG. 3. Total segment density profiles for chains of $M=8$ pinned at the left plane (a) and the individual segment density profiles for the segments pinned at the left plane [(b) and (c) the segment numbers are given in the figure]. The curves from bottom in (a) are for $R_C^*=0.1, 0.2, 0.4, 0.6, 0.8,$ and 0.9 . The curves in (b) and (c) are for $R_C^*=0.2$ and 0.9 , respectively. The inset to (a) shows the dependence of $\langle z_8 \rangle$ on R_C^* for $h_m=8\sigma_C$ (dashed lines) and for $h_m=19\sigma_C$ (solid line).

The inset to Fig. 3(a) illustrates the changes of the average position of the terminating segment, $\langle z_8 \rangle$, that can be considered as a measure of the stretching of the chains,

$$\langle z_8 \rangle = \int_0^{h_m/2} \rho_{s,8}^{(C)}(z') z' dz' / \int_0^{h_m/2} \rho_{s,8}^{(C)}(z') dz', \quad (9)$$

for two bilayers of $h_m=8\sigma_C$ [cf. Fig. 3] and of $h_m=19\sigma_C$. In the above $z'=z+h_m/2$. For $h_m=8\sigma_C$ the value $\langle z_8 \rangle$ attains a plateau for high R_C^* because the chains attached at the opposite planes prohibit their stretching. For $h_m=19\sigma_C$ the value of $\langle z_8 \rangle$ grows almost linearly with R_C^* .

We now proceed to the presentation of some results for a single bilayer in contact with a binary mixture of hard spheres of diameters $\sigma_1=\sigma_C$ and $\sigma_2=2\sigma_C$. The spheres of the diameter σ_2 cannot cross the bilayer center [cf. Eq. (4)], so the fluid on the left-hand side of the bilayer is just a one-component fluid of hard spheres of diameter σ_1 . Figures 4(a) and 4(b) show the structure of the bilayer and of the fluid in contact with the bilayer. The calculations are for $M=16$, $h_m=16\sigma_C$ and for $R_C^*=0.2$ (part a) and for $R_C^*=0.6$ (part b). There are two sets of curves in each figure. Black lines denote the results for the low-density mixture [$\rho_b^{(1)*}=\rho_b^{(1)}\sigma_1^3=\lim_{z\rightarrow\infty}\rho^{(1)}(z)\sigma_1^3=0.1$, $\rho_b^{(2)*}=\rho_b^{(2)}\sigma_1^3=\lim_{z\rightarrow\infty}\rho^{(2)}(z)\sigma_1^3=0.1$], whereas red lines are for the high-density mixture on the right-hand side of the bilayer ($\rho_b^{(1)*}=0.4$, $\rho_b^{(2)*}=0.4$).

The layers of first segments that are pinned at $z=-h_m/2$ and $z=h_m/2$ act like “partially hard walls,” and at both sides of the bilayer we observe well developed layered structure of the fluid. This effect is more pronounced for higher value of R_C^* . Because of the difference in the sizes of fluid molecules, the positions of consecutive local density maxima and minima for the species 1 do not coincide with those for the species 2. Moreover, because of the condition imposed by potential (4), there is an “artificial” hard wall at the bilayer center. When the total segment density inside of the bilayer is not very high [cf. Fig. 4(a)], we observe a well-pronounced peak of the fluid species 2 at $z=0$. This

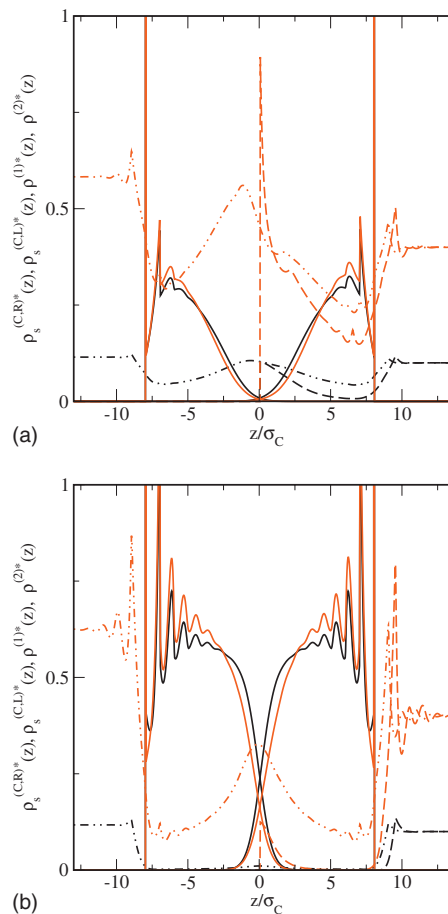


FIG. 4. Total segment density profiles for chains of $M=16$ pinned at the left and at the right plane (solid lines) and the fluid density profiles of the species 1 (dash-dotted lines) and of the species 2 (dashed lines). In (a) $R_C^*=0.2$, while in (b) $R_C^*=0.6$; in both cases $h_m=16\sigma_C$. Black lines are for $\rho_b^{(1)*}=\rho_b^{(2)*}=0.1$, while red lines are for $\rho_b^{(1)*}=\rho_b^{(2)*}=0.4$.

peak diminished with increasing R_C^* , and for $R_C^*=0.6$ [Fig. 4(b)] the concentration of the fluid particles of species 2 at the membrane center is low. Of course, one can impose the bilayer impenetrability condition in the form different than that given by Eq. (4). Then, for a given selection of potential (4) this peak can disappear. We return to this point below.

For the special model considered here an increase of the bulk density on the right-hand side of the bilayer results in an increase of densities of both fluid species inside the bilayer. The fluid molecules that are accumulated at the membrane center cause “tightening” the chains to the pinning plane. In the case of the systems shown in Figs. 4(a) and 4(b), the total segment density profiles of chains pinned to the left and right planes are almost symmetrical, although a careful inspection of the results indicates that the chains pinned at the right plane become more “tightened” to the pinning plane than those at the opposite side. However, breaking the symmetry of the total segment density profiles becomes more visible when the bulk density of fluid species on the right-hand side of the bilayer becomes much larger than the bulk density of species 1. This point is illustrated in Fig. 5 where we have displayed the density distributions obtained for the bilayer formed of 16-mers. We also see in Fig. 5 that confinement of fluid molecules inside the bilayer mostly influences the dis-

tribution of the outer segments of the chains (i.e., the segments that are located far from the pinned segment). Indeed, the change of the profiles of the $J=14$ and $J=16$ segments with the bulk fluid density on the right-hand side of the membrane is much more significant than the change of the distribution of the $J=2$ segments. We also find that the differences between the outer segments profiles for the chains pinned at the left and right sides of bilayer are much more pronounced than the differences between the profiles for the inner segments.

The structure of the fluid inside the bilayer is related to the imposed impenetrability condition, expressed by potential (4). One can consider different modifications of this potential. For example, one can assume that the Boltzmann factor for the molecules which cannot cross the bilayer, $\exp[-v^{(2)}(z)kT]$, decays linearly inside the bilayer from unity on its right-hand side to zero at $z=-h_m/2$, i.e.,

$$\exp[-v^{(2)}(z)kT] = \begin{cases} 1 & z \geq h_m/2 \\ (1/h_m)z + 1/2 & -h_m/2 \leq z \leq h_m/2 \\ 0 & z < -h_m/2. \end{cases} \quad (10)$$

Figure 6 shows the structure of a fluid at both sides and inside the bilayer when the impenetrability condition is given by Eq. (10). All remaining parameters characterizing the system are the same as those used to calculate the results shown in Fig. 5. We see that although the structure of the fluid inside the bilayer is now quite distinct from that presented in Fig. 5(a), but the density profiles of fluid molecules at both sides of the bilayer are almost identical as those obtained when the impenetrability condition is given by Eq. (4). Also, the total segment density profiles inside the bilayer in Figs. 5(a) and 6 do not differ significantly. In particular, the difference between the left- and right-hand side profiles is now much smaller than in Fig. 5(a).

Close similarity between the density profiles outside the bilayer for the systems shown in Figs. 5(a) and 6 results from relatively high value of R_C^* (in both cases $R_C^*=0.4$) and from the fact that all the interactions if the system are of hard-sphere type. In the presence of attractive forces between spherical species (i.e., segments and fluid molecules), the dependence of the structure outside the membrane on the imposed impenetrability condition may be significant, especially in the case of specific (e.g., associative) interactions between selected species.

We now consider two bilayers at a distance L apart. They form a kind of a slit-like pore that is filled by one-component fluid and outside the pore the fluid is a binary mixture of hard spheres. When L is large, the bilayers forming the walls of a “pore” are almost independent of each other. However, because of short-range hard-sphere interactions in the system, the influence of one bilayer on the structure of the second is weak, even for small L . This point illustrates Fig. 7 where we have plotted the profiles for bilayers separated by the distance of $L=4.5\sigma_C$ (black curves) and $L=\sigma_C$ (colored curves). In order to make comparisons easier, the origin of the z -axis (that is, originally located at the middle of the distance L) has been shifted by $L/2$, and only the part of the

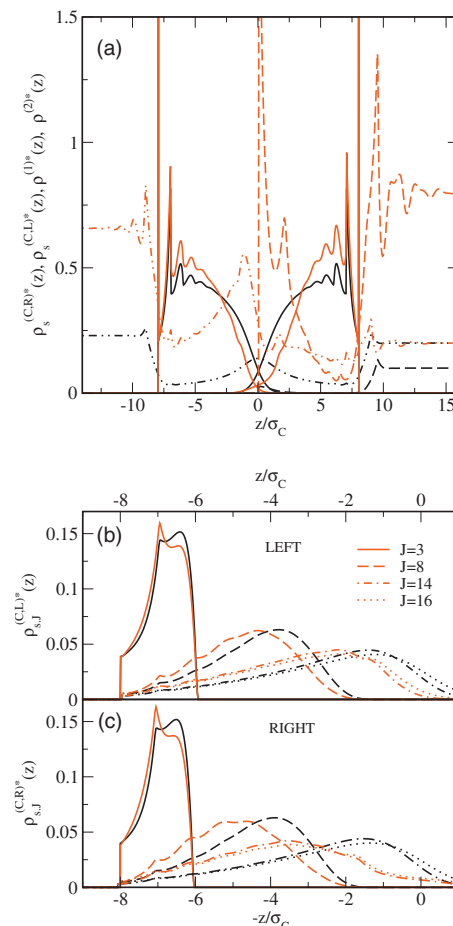


FIG. 5. (a) Total segment density profiles for chains of $M=16$ pinned at the left and at the right plane (solid lines) and the fluid density profiles of the species 1 (dash-dotted lines) and of the species 2 (dashed lines). The calculations are for $R_C^*=0.4$, $h_M=16\sigma_C$. Black lines are for $\rho_b^{(1)*}=0.2$ and $\rho_b^{(2)*}=0.1$, while red lines are for $\rho_b^{(1)*}=0.2$ and $\rho_b^{(2)*}=0.8$. [(b) and (c)] Individual segment density profile of for the chains pinned at the left (b) and right (c) side of the bilayer. The numbers of chains are given in the figure. In order to make a comparison easier, the mirror reflections of the right profiles are plotted.

profiles for $z \geq 0$ has been plotted. The calculations have been carried out keeping the total bulk density constant, $\rho_b^{(1)*} + \rho_b^{(2)*} = 0.8$. Part a is for $\rho_b^* = \rho_b^{(1)*} = \rho_b^{(2)*} = 0.4$, while part b is for $\rho_b^{(1)*} = 0.7$ and $\rho_b^{(2)*} = 0.1$.

The structure of the fluid outside the pore formed by two bilayers is practically independent of the distance L . Also, the structure of chains that are pinned at the right in Fig. 7 (i.e., outer, with respect to the pore formation) plane of the bilayer, as well as the structure of the impenetrable component 2 inside the bilayer, are almost independent of L . Of course, the bilayer-to-bilayer distance L influences the structure of the species 1 in the pore between two bilayers and inside the bilayers. When L decreases, the fluid is “squeezed out” of the space between the bilayers. At a constant ρ_b^* , the change of the structure of the fluid of species 1 is somewhat more pronounced if $\rho_b^{(1)*}$ is larger (and thus $\rho_b^{(2)*}$ is smaller), cf. Figs. 7(a) and 7(b).

The “squeezing” the fluid out of the pore leads to changes in the total segment density profiles, $\rho_s^{(C,L)*}(z)$, of the chains that are pinned at the left in Fig. 7 (i.e., inner) plane of

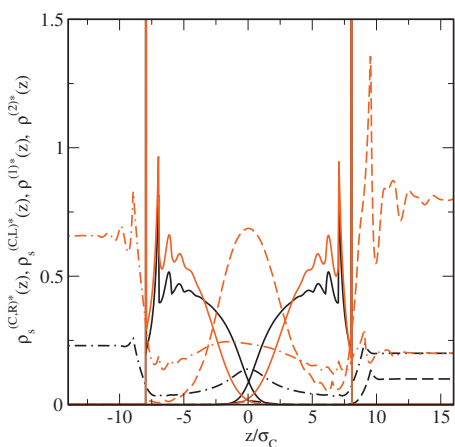


FIG. 6. The same as in Fig. 5(a), but now the impenetrability condition assures Eq. (10).

the bilayer. The most visible effect is the development of a small shoulder at the distances $0 < z - L/2 < 0.25\sigma_C$. Inspecting the density profiles of individual segments (they are not shown here for the sake of brevity), we have found that the development of this shoulder is almost solely due to the shift of the segments $J=2$ toward the bilayer center. The squeezing of the fluid molecules from the pore, however, does not cause stretching of the chain molecules. The stretching is hampered by the accumulation of fluid species 1 at the bilayer center.

We now proceed to the presentation of results for solvation forces. In the case of high values of R_C^* the closest approach distance between two bilayers equals to the minimum distance between two hexagonally packed layers, i.e., to $L_{\min} = \sqrt{(2/3)}\sigma_C \approx 0.82\sigma_C$. At that distance the repulsion between two layers filled with hexagonally ordered hard spheres becomes infinity. In general, for high values of R_C^* the behavior of the solvation force is expected to be qualita-

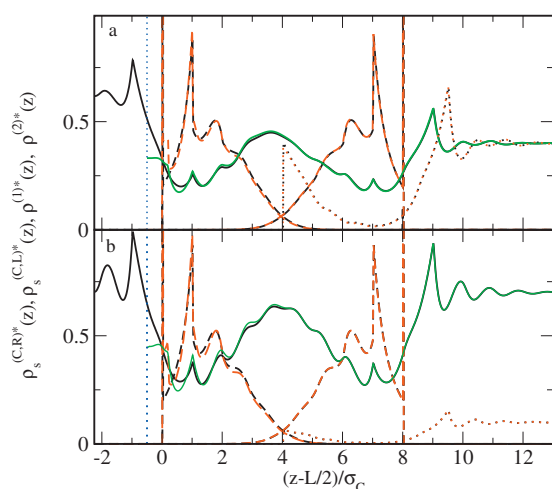


FIG. 7. Total segment density profiles (dashed lines), profiles of the component 1 (solid lines), and the profiles of the component 2 (dotted lines) for two bilayers at the distance $L=4.5\sigma_C$ (black curves) and $L=\sigma_C$ (colored curves). (a) is for $\rho_b^{(1)*} = \rho_b^{(2)*} = 0.4$ and (b) for $\rho_b^{(1)*} = 0.7$ and $\rho_b^{(2)*} = 0.1$. In all cases $M=8$, $h_m=8\sigma_C$, and $R_C^*=0.4$. Only one bilayer and a half the profiles between the two bilayers has been plotted. Vertical dotted blue line denotes the middle of the system comprising two bilayers at the distance $L=\sigma_C$ apart.

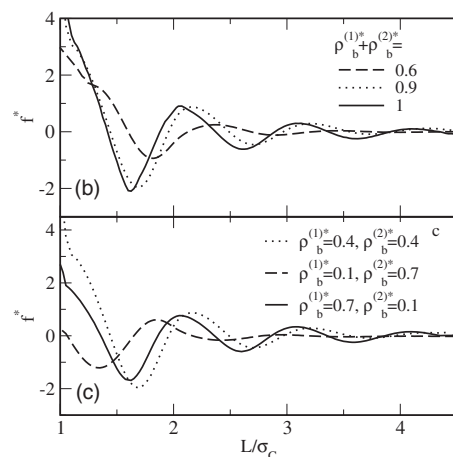
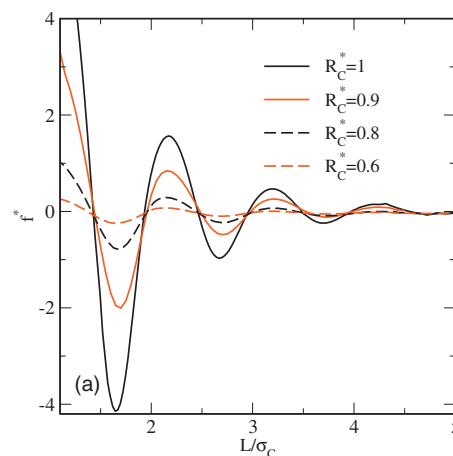


FIG. 8. (a) The dependence of the solvation force on R_C^* . The calculations are for $\rho_b^{(1)*} = \rho_b^{(2)*} = 0.4$. (b) The dependence of F^* on the total bulk fluid density, $\rho_b^{(1)*} + \rho_b^{(2)*}$, under the constraint $\rho_b^{(1)*} = \rho_b^{(2)*}$. The parameter R_C^* equals 0.9. (c) The solvation force at a constant total bulk density, $\rho_b^{(1)*} + \rho_b^{(2)*}$, but for different values of individual densities $\rho_b^{(1)*}$ and $\rho_b^{(2)*}$. The parameter R_C^* equals 0.9. All the calculations in (a)–(c) were carried out for $M=8$ and $h_m=8\sigma_C$.

tively similar to that observed for a fluid between two hard walls. On the other hand, for low R_C^* the walls formed by pinned chains are “soft,” so that the molecules of species 1 can cross it almost freely, since the number of segments that act like obstacles is low. Of course, for R_C^* approaching zero the solvation forces also vanish.

Figure 8(a) shows how the solvation force changes with R_C^* . The calculations have been carried out keeping the bulk densities constant, $\rho_b^{(1)*} = 0.4$ and $\rho_b^{(2)*} = 0.4$, and for the bilayers built of 8-mers, each bilayer of $8\sigma_C$ thick. It is evident that an increase of R_C^* leads to more pronounced oscillations. This effect is quite obvious, since for larger values of R_C^* the planes delimiting bilayers become “harder” for fluid particles. However, the locations of zeros of f^* depend only slightly on R_C^* . We recall that the distances L at which $f^*=0$ are the equilibrium distances between two bilayers that can move freely, i.e., when $f^*=0$ there is no attraction nor repulsion between the two bilayers.

Figure 8(b) illustrates how the solvation force changes when the total bulk density, $\rho_b^{(1)*} + \rho_b^{(2)*}$, is increased, under the constraint that $\rho_b^{(1)*} = \rho_b^{(2)*}$. Similarly as in Fig. 8(a) each bilayer is $8\sigma_C$ thick and is built of 8-mers. Now, R_C^* is kept

constant and equals 0.9. The increase of the total bulk density shifts systematically and reduces the period of oscillations as well as increases the repulsion between the two bilayers at small separation distances L . However, when the calculations of f^* are carried out keeping the total density $\rho_b^{(1)*} + \rho_b^{(2)*}$ constant, but changing the densities of permeable and nonpermeable components, the plots of f^* versus L do not change in a systematic way, see Fig. 8(a). One could think that an increase of the bulk density of the fluid component 1 should result in more pronounced oscillations. This is not the case, however. Considering the results plotted in Fig. 8(c) one should remember that the solvation force, as defined by Eq. (8), depends on the inner and outer contributions, as we have mentioned above. Unfortunately, the separation of these effects is impossible. An increase of the bulk density of the impenetrable component 2 leads to more pronounced peaks on the density profiles outside of each membrane and to the increase of the “intra bilayer” local density peak of this component, cf. Fig. 6(a). The development of the local density peaks of the component 2 always “pushes” one of the membrane toward another. The inner contribution, which is due to the component 1, can be either repulsive or attractive. Therefore, the combination of the inner and outer contributions can result in quite complex changes of f^* with the parameters describing the system.

Even for such very simple systems, as those studied in this work, the number of parameters that can influence the behavior of the solvation force is large. They are M , R_C , h_m , and the diameters of all spherical species. Of course, our study has not exhausted all important combinations of these parameters. The aim of our work has been to show some new possibilities that can be explored using density functional approaches.

One of the questions that can be asked concerns the accuracy of the proposed approach. In this work we did not perform comparisons of the theory with computer simulation results. However, in our previous works^{17,22,64,65} such comparisons were presented for quite similar systems. They have proved that the density functional theory is capable to predict reasonably well the structure of fluids in contact with a surface modified with pinned brushes, as well as in pores modified by pillars built of chains. Moreover, according to the applied approach the hard-sphere contribution to the free energy functional has been based on the Boublík–Moonsori–Carnahan–Starling–Leland equation of state. Because the latter theory is very accurate in predicting the dependence between the chemical potential and the bulk densities, the bulk densities on both sides of a single bilayer resulting from the proposed theory must be predicted correctly.

The proposed approach can be extended to more sophisticated systems. A straightforward extension is to take into account attractive interactions between all (or some selected) spherical species. In the simplest case the attractive interactions can be accounted for by employing a mean-field approximation, cf. Refs. 18, 22, and 23. Alternatively, the attractive force free energy contribution can be evaluated from the first order mean spherical approximation,^{66–68} or even using more sophisticated, weighted methods.^{69,70} The systems with attractive interactions between spherical species

may exhibit a quite complex phase behavior. Apart from the temperature dependent reorganization of the layers of chains, one can also expect the occurrence of the transitions in the fluid confined between two layers of chains, as well as surface phase transitions outside the bilayer, cf. Refs. 61 and 71. Moreover, one can apply a quite similar approach (cf. Ref. 29) to the case of systems involving charged species (ions and charged segments). Taking into account recent publications,^{12,20} also there are possible several modifications that would take into account more complex architecture of the pinned molecules and/or interactions between spherical species (i.e., fluid molecules and segments). However, the most important modifications that would allow for taking into consideration nonplanar pinning surfaces, and involving fluctuations of their geometry, are much more difficult to implement into the theory. This problem is currently under study in our laboratory.

ACKNOWLEDGMENTS

This work was supported by the Ministry of Science of Poland under Grant No. N N204 151237.

- ¹J. B. Hooper, J. D. McCoy, and J. D. Curro, *J. Chem. Phys.* **112**, 3090 (2000).
- ²Y.-X. Yu and J. Wu, *J. Chem. Phys.* **117**, 2368 (2002).
- ³P. Bryk and S. Sokółowski, *J. Chem. Phys.* **121**, 11314 (2004).
- ⁴Z. Ye, J. Cai, H. Liu, and Y. Hu, *J. Chem. Phys.* **123**, 194902 (2005).
- ⁵Y.-X. Yu, G.-H. Gao, and X.-L. Wang, *J. Phys. Chem. B* **110**, 14418 (2006).
- ⁶K. Bucior, J. Fischer, A. Patrykiewicz, R. Tscheliessnig, and S. Sokółowski, *J. Chem. Phys.* **126**, 094704 (2007).
- ⁷H. Chen, Z. Ye, J. Cai, H. Liu, Y. Hu, and J. Jiang, *J. Phys. Chem. B* **111**, 5927 (2007).
- ⁸K. Bucior, A. Patrykiewicz, S. Sokółowski, and O. Pizio, *Condens. Matter Phys.* **12**, 51 (2009).
- ⁹P. Bryk and L. G. MacDowell, *J. Chem. Phys.* **129**, 104901 (2008).
- ¹⁰D. Cao and J. Wu, *J. Chem. Phys.* **121**, 4210 (2004).
- ¹¹S. Tripathi and W. G. Chapman, *J. Chem. Phys.* **122**, 094506 (2005).
- ¹²A. Malijevsky, P. Bryk, and S. Sokółowski, *Phys. Rev. E* **72**, 032801 (2005).
- ¹³X. Xu, D. Cao, X. Zhang, and W. Wang, *Phys. Rev. E* **79**, 021805 (2009).
- ¹⁴Y. Ye, J. D. McCoy, and J. G. Curro, *J. Chem. Phys.* **119**, 555 (2003).
- ¹⁵D. P. Cao and J. Wu, *Langmuir* **22**, 2712 (2006).
- ¹⁶T. Jiang, Z. Li, and J. Wu, *Macromolecules* **40**, 334 (2007).
- ¹⁷M. Borówko, W. Rżysko, S. Sokółowski, and T. Staszewski, *J. Phys. Chem. B* **113**, 4763 (2009).
- ¹⁸A. Patrykiewicz, S. Sokółowski, R. Tscheliessnig, J. Fischer, and O. Pizio, *J. Phys. Chem. B* **112**, 4552 (2008).
- ¹⁹X. Xu and D. Cao, *J. Chem. Phys.* **130**, 164901 (2009).
- ²⁰X. Xu and D. Cao, *J. Chem. Phys.* **131**, 054901 (2009).
- ²¹O. J. Hehmyer, G. Arya, A. Z. Panagiotopoulos, and I. Szleifer, *J. Chem. Phys.* **126**, 244902 (2007).
- ²²Z. Sokółowska and S. Sokółowski, *J. Colloid Interface Sci.* **316**, 652 (2007).
- ²³M. Matusiewicz, A. Patrykiewicz, and S. Sokółowski, *J. Chem. Phys.* **127**, 174707 (2007).
- ²⁴C. N. Patra, R. Chang, and A. Yethiraj, *J. Phys. Chem. B* **108**, 9126 (2004).
- ²⁵H. Wang and A. R. Denton, *J. Chem. Phys.* **123**, 244901 (2005).
- ²⁶Z. D. Li and J. Z. Wu, *Phys. Rev. Lett.* **96**, 048302 (2006).
- ²⁷Z. D. Li and J. Z. Wu, *J. Phys. Chem. B* **110**, 7473 (2006).
- ²⁸T. G. Smagala, A. Patrykiewicz, S. Sokółowski, O. Pizio, and W. R. Fawcett, *J. Chem. Phys.* **128**, 024907 (2008).
- ²⁹P. van der Ploeg and H. J. C. Berendsen, *J. Chem. Phys.* **76**, 3271 (1982).
- ³⁰M. Milik, A. Kolinski, and J. Skolnick, *J. Chem. Phys.* **93**, 4440 (1990).
- ³¹N. Zheng, J. Geehan, and M. D. Whitmore, *Phys. Rev. E* **75**, 051922 (2007).

- ³²C. Ren and Y. Ma, *Phys. Rev. E* **80**, 011910 (2009).
- ³³A. L. Frischknecht and L. J. D. Frink, *Phys. Rev. E* **72**, 041924 (2005).
- ³⁴W. J. Koros and G. K. Fleming, *J. Membr. Sci.* **83**, 1 (1993).
- ³⁵R. E. Kesting and A. K. Fritzsche, *Polymeric Gas Separation Membranes* (Wiley, New York, 1993), pp. 61–233.
- ³⁶K.-L. Tung, K.-T. Lua, R.-C. Ruaan, and J.-Y. Lai, *Desalination* **192**, 391 (2006).
- ³⁷S. A. Safran, *Statistical Thermodynamics of Surfaces, Interfaces and Membranes* (Westview, Boulder, 1994).
- ³⁸H. T. Tien and A. Ottova-Leitmannova, *Planar Lipid Bilayers (BLMs) and Their Applications* (Elsevier, Amsterdam, 2003).
- ³⁹G. van Meer, D. R. Voelker, and G. W. Feigenson, *Nat. Rev. Mol. Cell Biol.* **9**, 112 (2008).
- ⁴⁰G. Brannigan, L. C.-L. Lin, and F. L. H. Brown, *Eur. Biophys. J.* **35**, 104 (2006).
- ⁴¹W. L. Ash, M. R. Zlomislic, E. O. Oloo, and D. P. Tieleman, *Biochim. Biophys. Acta* **1666**, 158 (2004).
- ⁴²S. Murad and J. Powles, in *Computational Methods in Surface And Colloid Science*, edited by M. Borówko (Dekker, New York, 2000), Chap. 16.
- ⁴³S. J. Marrink, H. J. Risselada, S. Yefimov, D. P. Tieleman, and A. H. de Vries, *J. Phys. Chem. B* **111**, 7812 (2007).
- ⁴⁴G. Brannigan, P. F. Phillips, and F. L. H. Brown, *Phys. Rev. E* **72**, 011915 (2005).
- ⁴⁵J. P. Ulmschneider and M. B. Ulmschneider, *J. Chem. Theory Comput.* **3**, 2335 (2007).
- ⁴⁶P. J. Bond and M. S. P. Sansom, *J. Am. Chem. Soc.* **128**, 2697 (2006).
- ⁴⁷S. J. Paddison and J. A. Elliott, *J. Phys. Chem. A* **109**, 7583 (2005).
- ⁴⁸W. Soliman, S. Bhattacharjee, and K. Kaur, *Langmuir* **25**, 6591 (2009).
- ⁴⁹M. Bloom, E. Evans, and O. G. Mouritsen, *Q. Rev. Biophys.* **24**, 293 (1991).
- ⁵⁰A. Ben-Shaul, I. Szleifer, and W. M. Gelbart, *J. Chem. Phys.* **83**, 3597 (1985).
- ⁵¹I. Szleifer, A. Ben-Shaul, and W. M. Gelbart, *J. Chem. Phys.* **85**, 5345 (1986); **86**, 7094 (1987).
- ⁵²D. Harries and A. Ben-Shaul, *J. Chem. Phys.* **106**, 1609 (1997).
- ⁵³T. Sintès and A. Baumgartner, *Physica A* **249**, 571 (1998).
- ⁵⁴L. Whitehead, C. M. Edge, and J. W. Essex, *J. Comput. Chem.* **22**, 1622 (2001).
- ⁵⁵S. Y. Lim, M. Sahimi, T. T. Tsotsis, and N. Kim, *Phys. Rev. E* **76**, 011810 (2007).
- ⁵⁶D. Q. Vu, W. J. Koros, and S. J. Miller, *J. Membr. Sci.* **211**, 311 (2003).
- ⁵⁷H.-J. Butt, B. Cappella, and M. Kappl, *Surf. Sci. Rep.* **59**, 1 (2005).
- ⁵⁸F. Dong, B. Olsen, and N. A. Baker, *Methods Cell Biol.* **84**, 843 (2008).
- ⁵⁹O. Pizio, L. Pusztai, Z. Sokołowska, and S. Sokołowski, *J. Chem. Phys.* **130**, 134501 (2009).
- ⁶⁰P. Bryk, O. Pizio, and S. Sokołowski, *J. Phys. Chem. B* **103**, 3366 (1999).
- ⁶¹D. Boda, D. Henderson, R. Rowley, S. Sokołowski, *J. Chem. Phys.* **111**, 9382 (1999).
- ⁶²Y.-X. Yu and J. Wu, *J. Chem. Phys.* **118**, 3835 (2003).
- ⁶³P. Bryk and S. Sokołowski, *J. Chem. Phys.* **120**, 8299 (2004).
- ⁶⁴O. Pizio, M. Borówko, W. Rzyśko, T. Staszewski, and S. Sokołowski, *J. Chem. Phys.* **128**, 044702 (2008).
- ⁶⁵M. Borówko, W. Rzyśko, S. Sokołowski, and T. Staszewski, *J. Chem. Phys.* **126**, 214703 (2007).
- ⁶⁶Y. P. Tang, *J. Chem. Phys.* **118**, 4140 (2003).
- ⁶⁷Y. Tang and J. Wu, *Phys. Rev. E* **70**, 011201 (2004).
- ⁶⁸P. Bryk, W. Rzyśko, A. Malijevsky, and S. Sokołowski, *J. Colloid Interface Sci.* **313**, 41 (2007).
- ⁶⁹B. Peng and Y.-X. Yu, *J. Phys. Chem. B* **112**, 15407 (2008).
- ⁷⁰Y.-X. Yu, *J. Chem. Phys.* **131**, 024704 (2009).
- ⁷¹P. Bryk, J. Reszko-Zygmunt, A. Patrykiewicz, and S. Sokołowski, *Mol. Phys.* **96**, 1509 (1999).